Eur. Phys. J. D **14**, 323–330 (2001)

THE EUROPEAN PHYSICAL JOURNAL D

EDP Sciences
© Società Italiana di Fisica
Springer-Verlag 2001

Metastable fragmentation of silver bromide clusters

J.-M. L'Hermite[a], F. Rabilloud, L. Marcou, and P. Labastie

Laboratoire CAR/IRSAMC[b], Université Paul Sabatier, 118 route de Narbonne, 30062 Toulouse Cedex, France

Received 9 November 2000 and Received in final form 25 January 2001

Abstract. The abundance spectra and the fragmentation channels of silver bromide clusters have been measured and analyzed. The most abundant species are $Ag_nBr^+_{n-1}$ and $Ag_nBr^-_{n+1}$ and $Ag_{14}Br^+_{13}$ is a magic number, revealing their ionic nature. However, some features depart from what is generally observed for alkali-halide ionic clusters. From a certain size, $Ag_nBr^+_{n-1}$ is no more the main series, and $Ag_nBr^+_{n-2,3}$ series become almost as important. The fast fragmentation induced by a UV laser makes the cations lose more bromine than silver ions and lead to more silver-rich clusters. Negative ions mass spectra contain also species with more silver atoms than required by stoichiometry. We have investigated the metastable fragmentation of the cations using a new experimental method. The large majority of the cations release mainly a neutral Ag_3Br_3 cluster. These decay channels are in full agreement with our recent *ab initio* DFT calculations, which show that Ag^+–Ag^+ repulsion is reduced due to a globally attractive interaction of their d orbitals. This effect leads to a particularly stable trimer $(AgBr)_3$ and to quasi-planar cyclic structures of $(AgBr)_n$ clusters up to $n = 6$. We have shown that these two features may be extended to other silver halides, to silver hydroxides $(AgOH)_n$, and to cuprous halide compounds.

PACS. 36.40.Qv Stability and fragmentation of clusters

1 Introduction

Silver bromide has been extensively studied for many years at the bulk level due to its implication in the photographic process. It is known today that the formation of the latent image consists in the aggregation of small silver clusters (Ag_4 at least) at the surface of silver bromide microcrystals [1]. In the development process, these clusters act as catalyst for the reduction of the silver cations to atoms [2,3]. Nevertheless, the very first step of photography is not understood yet: what is the process leading from photoabsorption to the small silver clusters? All the proposed mechanisms are more or less based on the Gurney and Mott theory [4]: there would be an accumulation, in a surface defect, of silver ions and photoelectrons, leading finally to small silver clusters. The various theories differ in the charge state of the intermediate steps; one can either first neutralize silver cations and then put them together, or first gather ions and then neutralize the resultant cluster, or even form an anionic cluster and then trap silver cations. The problem with these theories is that the calculated efficiency of the processes is smaller by orders of magnitude than the measured one. Actually, it is surprising, owing to the importance of the subject, that the knowledge of silver bromide at the molecular level is so poor. At the time we started to study silver bromide clusters the spectroscopy of the AgBr molecule was hardly known.

On the other hand, several studies of ionic clusters have been published. They have led to a general understanding of alkali halide quasi-stoichiometric clusters, which can be used as a starting point for the study of the more complex silver halide clusters. In this paper, we present fragmentation data, which give some insight into the behavior of silver and bromine atoms interacting with silver bromide stoichiometric salt.

Only anionic and cationic silver bromide clusters have been studied because the ionization potential of neutral species, estimated to more than 7 eV [5], is not accessible to commonly available lasers. Abundance spectra are studied in the next section. In the following section, metastable fragmentation channels are analyzed using our newly developed method and compared with recent *ab initio* DFT results [5], in the frame of the RRK (Rice, Ramsperger, Kassel) [6,7] statistical decay model and the evaporative ensemble [8].

We will finally show that some previously reported properties of silver chloride, silver hydroxide and copper halides (CuBr, CuCl) may be understood if one consider that the specificity of silver bromide clusters may be extended to other isoelectronic systems.

2 Experiment

The experimental setup is shown in Figure 1. It has already been detailed elsewhere [9,10]. The source is based on laser vaporization of a silver bromide rotating rod

[a] e-mail: jmarc@yosemite.ups-tlse.fr
[b] UMR 5589 du CNRS

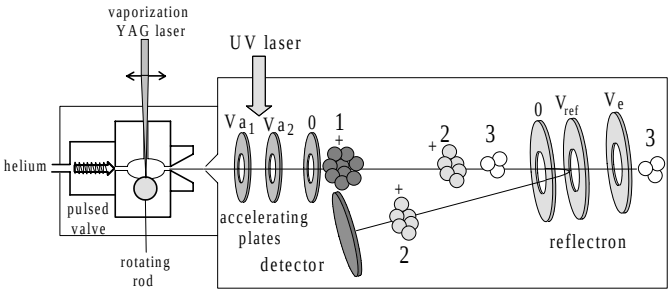

Fig. 1. Experimental setup. The silver bromide clusters are produced by laser vaporization of a silver bromide rod. The UV laser is used only in fast fragmentation experiments. Metastable fragmentation is pictured: (1) charged parent, (2) charged fragment, (3) neutral fragment.

using a 532 nm Nd:YAG laser. Clusters are seeded in helium gas and mass selected in a Reflectron-Time-Of-Flight (RETOF) mass spectrometer. The ions created in the source are accelerated by the pulsed high voltage of one or two of the first plates of the Wiley-Mc Laren device. A reflectron is used both to improve the mass resolution and to analyze the metastable fragmentation in the field-free region. Our source produces clusters at vibrational temperature close to the room temperature [11], leading to spontaneous fragmentation of silver bromide clusters in the field-free region of the mass spectrometer without any further heating. We developed a new method for measuring the fragmentation patterns, which has been presented in details elsewhere [12]. Briefly, it consists in scanning the voltage of the end plate of the reflectron, and then plotting the evolution of the time of flight peaks as a function of the inverse of this voltage. The points are aligned on straight lines. Each straight line corresponds to a given (parent, fragment) couple. The intersection with the Y-axis corresponds to an infinite repulsive voltage: in this case, the cluster spent no time in the reflectron. Knowing that the time of flight spent out of the reflectron depends only on the mass of the parent, this quantity can unambiguously be deduced from the intersection time. It is also easy to show that the slope of the straight line is proportional to the mass of the fragment. We have two parameters (the intersection point and the slope) to determine two unknowns (the masses of the parent and the fragment): the masses of the parents and the fragments are thus unambiguously determined.

3 Results and discussion

3.1 Mass spectra

Both silver and bromine atoms have two natural isotopes, respectively ^{107,109}Ag and ^{79,81}Br, whose natural abundance is about 50%/50%, so that the mass peak corresponding to a given Ag_pBr_q cluster is split into $(p+q+1)$ components with a binomial intensity distribution. When the isotopic mass peaks are resolved, one can integrate over the mass peaks associated with a given cluster size; it

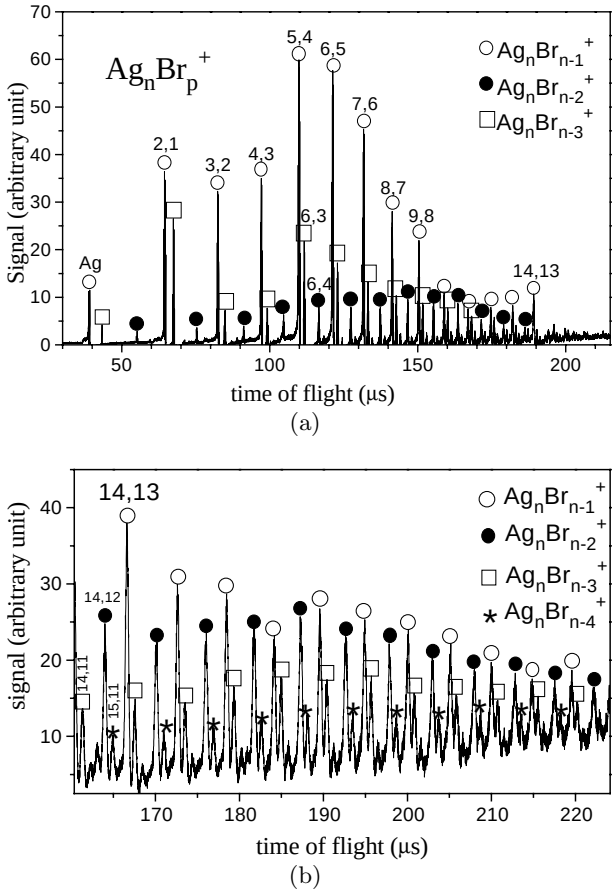

Fig. 2. Mass spectra of small (a) and larger (b) positively charged silver bromide clusters. The numbers n, p above some peaks refer to the number n of silver and p of bromine of the corresponding cluster.

is obviously not possible for unresolved spectra. We chose to apply the following simple correction to both resolved and unresolved spectra. Since the width of the binomial distribution is proportional to $\sqrt{p+q}$, the height of the mass peak is proportional to $I/\sqrt{p+q}$ where I is the total integrated intensity for this composition. For a given stoichiometry (p/q ratio), the correction is proportional to $\sqrt{m}$, with m the mass of the cluster. The clusters under study have almost stoichiometric composition, so that we can consider that the correction is roughly proportional to $\sqrt{m}$ for all the clusters. Thus all the mass spectra presented in this paper have been multiplied by $\sqrt{m}$, in order to show peak intensities closer to the real abundance.

3.1.1 Positive ions

Figures 2a and 2b display two mass spectra of positively charged silver bromide clusters. The accelerating voltage pulse of the mass spectrometer occurs later for Figure 2b, so that larger sizes are observed. The most intense series corresponds to stoichiometric species $Ag_nBr_{n-1}^+$ (we consider here and in the following as "stoichiometric"

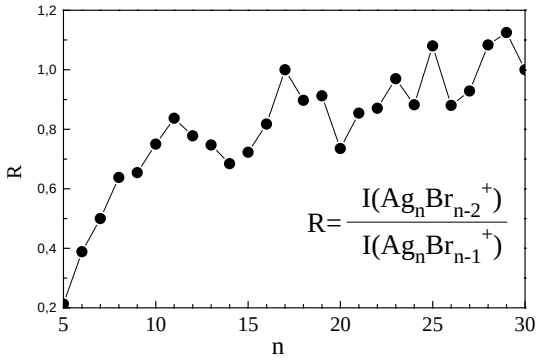

Fig. 3. Ratio of the abundance of $Ag_nBr^+_{n-2}$ and $Ag_nBr^+_{n-1}$.

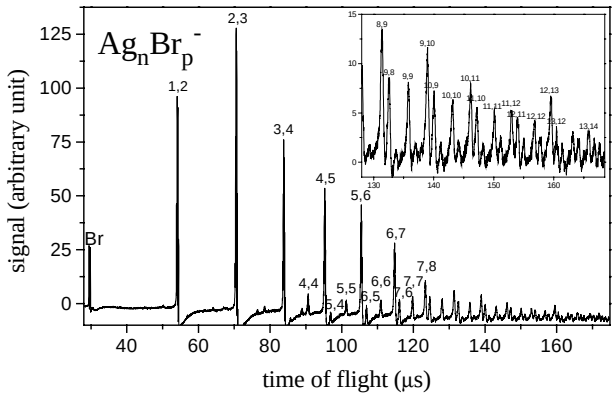

Fig. 4. Mass spectra of negatively charged silver bromide clusters. The numbers n, p above some peaks refer to the number n of silver and p of bromine of the corresponding cluster.

clusters with no excess electrons). Moreover, $Ag_{14}Br^+_{13}$ appears with a larger intensity than its neighbors. It denotes probably a $3 \times 3 \times 3$ cubic structure known to be particularly stable for all ionic clusters with no exception, to the best of our knowledge [9,10]. These features, already observed in previous experiments [13,14], reveal that they are at least partially ionic. On the one hand, we will see in the following that some covalent character strongly influence the structure of smaller clusters. On the other hand, bulk silver bromide is known to exhibit many characters of ionic compounds (crystal structure, conductivity) [15,16]: there should be a critical size from which the structures are no more influenced by covalence. It raises the question of whether the ionic character has already become dominant for $Ag_{14}Br_{13}$. Unfortunately, we are not able to give a final answer to this question. *Ab initio* calculations cannot be carried out for clusters large enough to determine the critical size [5]. It has only been shown that the cubic isomer of $Ag_{14}Br_{13}$ is stable, but not that it is the lowest isomer.

More bromine-deficient series are also detected, corresponding to $Ag_nBr^+_{n-2,n-3,n-4}$ (Fig. 2b). The ratio of the relative abundance of $Ag_nBr^+_{n-2}$ and $Ag_nBr^+_{n-1}$ are represented in Figure 3. This ratio first increases up to $n = 11$, for which the $(n, n-2)^+$ cluster is almost as stable as the stoichiometric one, and then decreases to reach an expected minimum for $Ag_{14}Br^+_{13}$. There is globally a constant increase of the relative abundance of $Ag_nBr^+_{n-2}$ cluster, which reach the same intensity as the stoichiometric series for $n > 25$. The presence of $Ag_nBr^+_{n-2}$, $Ag_nBr^+_{n-3}$ and $Ag_nBr^+_{n-4}$ has not been clearly observed in the experiments mentioned above [13,14]. It may be due to the different conditions of aggregation in the source, but should also be explained by a higher temperature of their clusters. As a matter of fact, metal rich alkali halide cations are generally produced more easily when the temperature of the source is lowered [17]. This seems to be confirmed by our experiments where these series disappear when the clusters are heated with a laser. The large intensity of $Ag_5Br^+_4$, also observed in [13], is unusual for "regular" ionic clusters [18]. Actually, we will see later that this high intensity is not due to a particular stability of $Ag_5Br^+_4$, but rather to the particular fragmentation channels that lead to its formation.

3.1.2 Negative ions

Figure 4 presents a relative abundance spectrum of silver bromide anions. The main series $Ag_nBr^-_{n+1}$ is stoichiometric. However, as in the case of cations, two other series of comparable intensity, namely $Ag_nBr^-_n$ and $Ag_nBr^-_{n-1}$, appear for the largest observed size. It denotes once again the probable ionic nature of quasi-stoichiometric silver bromide clusters, but also the stability of metal-rich species.

3.1.3 Fast fragmentation experiment

The positively charged clusters underwent an irradiation with the rather intense ($\approx 10^6$ W/cm^2) beam of a Nd:YAG laser at 266 nm or 355 nm. We recorded mass spectra under normal conditions. While proceeding in such a way, the resulting spectra reveal the fast fragmentation, which occurs immediately after the interaction with the laser, in a time scale smaller than a few nanoseconds. A typical spectrum of irradiated clusters is shown in Figure 5. There are no major differences between the spectra obtained at 266 nm and 355 nm. It means that there is no resonant excitation and that the observed changes are probably only due to the heating of the clusters. The spectrum of Figure 5 is very different from the one of Figure 2. The $Ag_nBr^+_{n-2}$ series almost completely disappear, and new series are formed between the stoichiometric clusters. Starting from the stoichiometric cluster $Ag_nBr^+_{n-1}$, the following peaks can be deduced from the previous ones by adding a silver atom and removing a bromine atom. One can observe, for example, the series $Ag_5Br^+_4$, $Ag_6Br^+_3$, $Ag_7Br^+_2$, Ag_8Br^+, Ag^+_9. The quasi-stoichiometric parent clusters have a higher propensity (summed over all the open channels) to lose bromine atoms than silver atoms or stoichiometric fragments. The stable clusters resulting from fragmentation have always an even number of electrons, even for clusters with a few excess metal atoms, as if there were a segregation of an ionic part and a metallic part responsible for the characteristic even/odd stability alternation. A monotonic evolution of

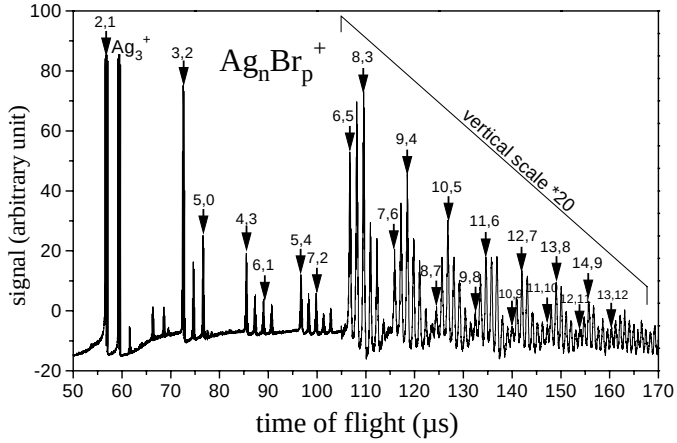

Fig. 5. Mass spectrum of silver bromide cations irradiated with the intense beam of a Nd:YAG laser at 355 nm: more bromine deficient clusters appear. The numbers n, p above some peaks refer to the number n of silver and p of bromine of the corresponding cluster.

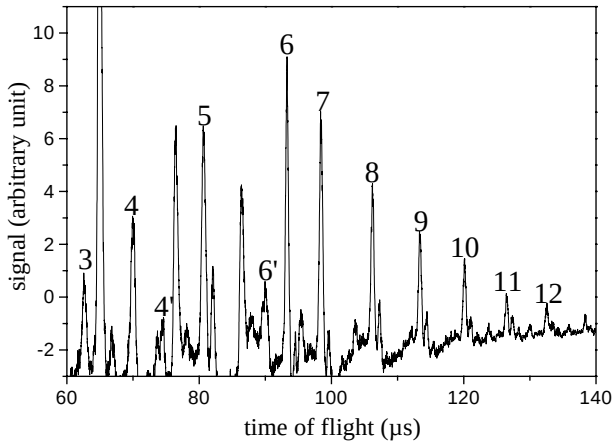

Fig. 6. Fragmentation spectrum of silver bromide clusters. The reaction corresponding to each peak is detailed in Table 1. The large majority of the most intense peaks (4, 5, 6', 7, 8, 9, 10, 11, 12) correspond to the evaporation of Ag_3Br_3.

the stability of the clusters within a series would probably lead to a monotonic decrease of the intensities from $Ag_nBr_{n-1}^+$ to Ag_p^+. Indeed, it is not what is observed. For all series, from $Ag_8Br_3^+$ to $Ag_{14}Br_9^+$, the most intense peaks are $Ag_nBr_{n-5}^+$. They may also be described as $(Ag_{n-4}Br_{n-5})^+ + Ag_4$ or $(Ag_{n-5}Br_{n-5}) + Ag_5^+$ in a segregated picture. For clusters larger than $Ag_{14}Br_{13}^+$, the most stable products are $(Ag_nBr_{n-1})^+Ag_8$. Ag_4 and Ag_8 are known to be very stable: there is a sudden increase in the binding energy from Ag_3 to Ag_4 (+36% [19]) and the binding energy presents a maximum for Ag_8 [20]. This suggests that Ag_4 and Ag_8 behave as if they were isolated, in other words that they are segregated. Although the mechanism of formation is probably different, it looks like what occurs in the photographic process, in which one has also a photo-induced segregation of Ag_4 on an ionic substrate.

These results on fast fragmentation might appear at a first glance in contradiction with the results of the metastable fragmentation experiments, which revealed the preferred evaporation of trimers $(AgBr)_3$. However, the two experiments are not contradictory: here the internal energy of the clusters is much higher than in metastable fragmentation experiments where the internal energy is thermal (roughly at room temperature), and many additional decay channels are open. The size distribution of fast fragmented clusters shifted toward small masses is consistent with the loss of trimers, which is likely to remain one important open channel. It is difficult to go further in the analysis of the fragmentation of clusters with high internal energy. First, it would require the calculation of non stoichiometric clusters (particularly metal-rich clusters); second, low-lying excited electronic states should be taken into account. This last requirement does not mean that evaporation processes necessarily involve direct photo-induced excitation (although it is not excluded), but that the internal energy of the hot cluster is large enough to possibly populate these states.

3.2 Metastable fragmentation

In the experiment described in the previous paragraph, it was impossible to know the fragmentation paths which lead to the observed species. Several methods are known to be able to analyze the metastable fragmentation which occurs in the field-free region of a RETOF mass spectrometer [12]. Unfortunately, it is very difficult, and sometimes impossible, in this kind of experiment to raise ambiguities in determining the fragmentation channels. That is why we were to develop a novel method, which is able to measure without any ambiguity the couples (parent, fragment) [12]. It has been applied to silver bromide positively charged clusters under experimental conditions where the initial distribution is close to the one of Figure 2. Positively charged fragments were detected. Clusters were not heated with a laser in the accelerating zone, but we slightly increased the fluence of the vaporization laser. Thus clusters underwent spontaneous fragmentation because of their higher initial internal energy.

3.2.1 Fragmentation channels

On the fragmentation spectrum of Figure 6, the largest peaks come from the fragmentation of $Ag_nBr_{n-1}^+$ clusters. Let us recall that in such experiments V_e is set to 0 and V_{ref} is kept smaller than V_{a_2} (see Fig. 1), so that clusters which did not undergo fragmentation are not reflected (their kinetic energy is larger than the potential barrier) and thus not detected. The assignment of the corresponding fragmentation reactions appears in Table 1 together with the calculated dissociation energies when available and the measured fragmentation rates. It is very striking that the most important decay channels are often $Ag_nBr_{n-1}^+ \rightarrow Ag_{n-3}Br_{n-4}^+ + Ag_3Br_3$. Actually, the detected fragment is the charged one $Ag_{n-3}Br_{n-4}^+$, and we can only infer from the experiment that the parent lose 3 silver

parent	fragments	frag. rate (%)	D_n (eV)	Peak n°(fig.5)
$2,1^+$	$1,0^+$ + 1,1	0.15	2.095	
$3,2^+$	$2,1^+$ + 1,1	1.9	1.647	3
$4,3^+$	$1,0^+$ + **3,3**	1.2	1.660	4
	$3,2^+$ + 1,1	1.5	1.783	4'
$5,4^+$	$2,1^+$ + **3,3**	1.2	1.663	5
$6,5^+$	$5,4^+$ + 1,1	6.3	Δ*	6
	$3,2^+$ + **3,3**	1.2	Δ+0.016	6'
$7,6^+$	$4,3^+$ + **3,3**	5.8		7
$8,7^+$	$5,4^+$ + **3,3**	9.8		8
$9,8^+$	$6,5^+$ + **3,3**	11.5		9
$10,9^+$	$7,6^+$ + **3,3**	12.8		10
$11,10^+$	$8,7^+$ + **3,3**	12		11

Table 1. Lowest fragmentation channels of $Ag_nBr^+_{n-1}$. D_n are the calculated dissociation energies from reference [5]. Experimental and calculated lowest channels are the same. * The ground state energy of $Ag_6Br^+_5$ is unknown. Nevertheless, it is possible to calculate the dissociation energies to a constant Δ.

atoms and 3 bromine atoms. However, as it will be demonstrated in the next paragraph, our theoretical work suggests that these 6 atoms be released together as a trimer $(AgBr)_3$. Non-stoichiometric clusters $Ag_nBr^+_{n-2,3,5}$ follow the same scheme and evaporate also often preferentially $(AgBr)_3$. The evaporation (we should rather say "fission" in this case) of trimers may be extended to some copper and silver halides whose vapors are known to contain a non-negligible fraction of trimers [21,22]. Similar evaporation properties have also been suggested (but not directly observed) for silver hydroxides $Ag_n(OH)^+_p$ [23–25]. This will be discussed in the last section.

The stability, the structural and electronic properties of small neutral and charged clusters $Ag_nBr_{p=n,n-1}$ ($n = 1-6$) have been investigated in the framework of *ab initio* DFT (B3LYP) calculations [5]. We will just mention here the main conclusions, in relation with our measured fragmentation patterns. First, it has been shown that the silver bromide clusters are not fully ionic (the Mulliken population analysis gives an ionicity of 56% for AgBr, and only 30% for $(AgBr)_3$ [5]). In small clusters, the binding energy is only partially assumed by the coulombic interaction between plus and minus charges. A non-negligible fraction of it is due to molecular orbitals involving d atomic orbitals of silver and p atomic orbitals of bromine. This kind of bonding, associated to the high polarizability of the bromine anion, tends to bend Ag–Br–Ag sub-structures with an angle of about 100°, whereas, on the contrary, the linear Br–Ag–Br configuration is favored. Two important implications of this feature are first that the ground state structures are different from the ones encountered in general for ionic clusters (Fig. 7), second, since there are attractive 3-body interactions between silver ions, that clusters with several silver atoms are more stable than expected. For this last reason, Ag_3Br_3 is especially stable and is one of the products of all the lowest fragmentation channels of $Ag_nBr^+_{n-1}$ ($n > 3$, of course). $Ag_6Br^+_5$ is an exception and evaporates preferentially AgBr. Nevertheless, the fragmentation into Ag_3Br_3 also occurs since its dissociation energy is very close (+0.016 eV only, see Tab. 1). It is confirmed in the experiment where the two corresponding peaks are detected (see Fig. 6). Two similar fragmentation channels

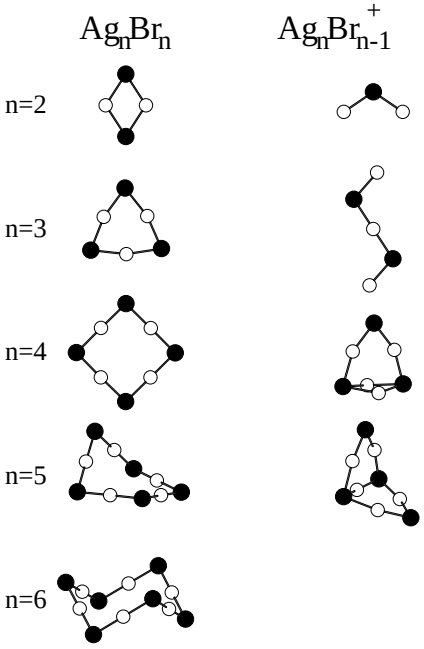

Fig. 7. Ground state structure of Ag_nBr_n and $Ag_nBr^+_{n-1}$ as determined in DFT (B3LYP) calculations [5]. Black circles are bromine, white circles are silver.

are observed for $Ag_4Br^+_3$, which can release either AgBr or $(AgBr)_3$. This is in good agreement with the calculated dissociation energies which are very close for these two channels. The observed fragmentation channels for the smallest clusters Ag_2Br^+ and $Ag_3Br^+_2$, which evaporate respectively a silver cation and a neutral silver bromide dimer, are also the lowest calculated ones. The perfect agreement of the measurements and the calculations on purely energetic grounds suggests that there is no potential barrier along the dissociation pathways. It is not really surprising since silver bromide clusters are more "floppy" than pure ionic clusters such as alkali-halides. There is always a balance between the coulombic forces which favor linear Ag–Br–Ag substructures and the polarization of bromine and the mixing of the d orbitals of silver cations that both bend these substructures, with only small energy differences between the two shapes.

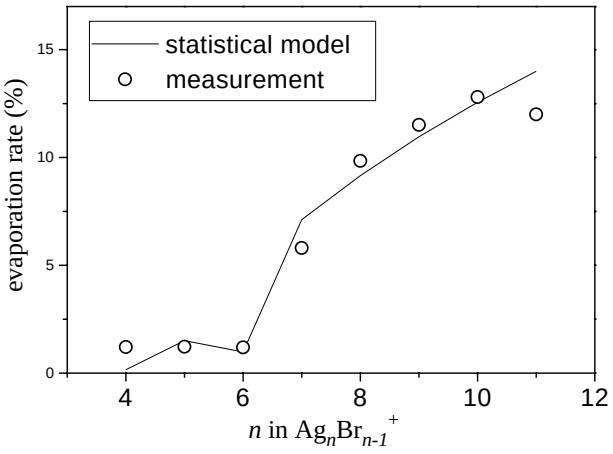

Fig. 8. Measured (circles) and calculated (line) evaporation rates of $Ag_nBr^+_{n-1}$ clusters into $Ag_{n-3}Br^+_{n-4} + Ag_3Br_3$.

3.2.2 Fragmentation rates

The fragmentation rates have been measured for all channels by dividing the signal of a given peak of the fragmentation spectrum (such as the one of Fig. 6) by the signal of the parent in a spectrum recorded under normal RETOF operation mode. The isotopic splitting is not resolved in fragmentation experiments. The abundance of a cluster is deduced from the height of the corresponding peak by considering a binomial distribution over the possible isotopes. One must also take care of the fact that in a RETOF mass spectrometer the intensity, say I'_n, of a peak reflects the abundance of the corresponding cluster X_n at the entrance of the reflectron. Let F_n be the sum of the intensities of all the peaks with X_n as parent in the fragmentation spectrum. F_n is the total fragmentation rate of X_n. The initial population I_n (at the end plate of the accelerating stage) of the cluster X_n is thus equal to $I_n = I'_n + F_n$. The fragmentation rate $F_{n\to n'}$ for a particular channel ($X_n \to X'_n$) with a peak intensity $I_{n\to n'}$ is given by:

$$F_{n\to n'} = \frac{I_{n\to n'}}{I_n} = \frac{I_{n\to n'}}{(I'_n + F_n)} \cdot \qquad (1)$$

The quantities $F_{n\to n'}$ are plotted in Figure 8 for $X_n = Ag_nBr^+_{n-1}$ and $X'_n = X_n - Ag_3Br_3$. The intensities $I_{n\to n'}$ can be taken from any of the fragmentation spectrum on which they appear, since they do not vary from one voltage $V_{\rm ref}$ to another [12].

The shape of the evolution of $F_{n\to n'}$ *versus* n is compared to *ab initio* calculations in the frame of a very simple statistical decay model based on the evaporative ensemble theory [8] of Klots using the RRK fragmentation rates [6,7]. Actually, the evaporation of large fragments such as Ag_3Br_3 from small clusters would certainly require a more sophisticated treatment (that does not exists at this time to our knowledge), but we intentionally chose one of the simplest statistical decay models, just in order to know roughly if the experiment was consistent with the calculations. The evaporation rate $K(n, E^*_n)$ is given by the Kassel formula:

$$K(n, E^*_n) = \nu_0[(E^*_n - D_n)/E^*_n]^{(3n-7)} \qquad (2)$$

E^*_n is the internal energy of the parent, D_n the dissociation energy for the considered channel, and ν_0 a mean vibrational frequency. n is the total number of atoms in the cluster, it is equal to $2m-1$ for Ag_mBr_{m-1}. We gave up the usual degeneracy factor, in general taken proportional to the surface of the cluster, because it is not a reliable factor to our mind in the case of small clusters (all atoms are at the surface in clusters of these sizes!). ν_0 is constant, equal to 1.8×10^{12} s^{-1}. It is the only parameter that we adjusted in order to compare rates to experiment. D_n was taken from the *ab initio* DFT calculations (see Tab. 1) for the clusters smaller than $Ag_6Br^+_5$. Considering the weak variation of D_n with n (see Tab. 1), we took a constant value $D_n = 1.66$ eV for the larger clusters for which it has not been calculated. The initial internal energies E^*_n were deduced from the evaporative ensemble model, associated with the RRK formula, applied to the evolution of the temperature of the clusters from the source to the accelerating stage of the mass spectrometer. This model gives a maximum value $E_{\rm max}$ and a minimum value $E_{\rm min}$ of E^*_n. E^*_n was taken as $(E_{\rm max} + E_{\rm min})/2$. The branching ratios for the reactions involving $Ag_6Br^+_5$ or $Ag_4Br^+_3$ (which have both two important dissociation channels) are directly taken from the experiment as the ratio of the height of the corresponding peaks.

The calculated dissociation rates into Ag_3Br_3 are in rather good agreement with the experimental results (Fig. 8): the fragmentation rate, in the order of a few percent for $n \leq 6$, sharply increases from $n = 7$ to reach about 13% for $n = 10$. The low dissociation rate of $Ag_6Br^+_5$ into $(AgBr)_3$ is easy to understand since there are two quasi-degenerate channels with a higher probability for the release of a molecular monomer AgBr. The large abundance of $Ag_5Br^+_4$ in the mass spectra recorded under normal conditions is also easily understood if one consider that the observed clusters come from the dissociation of larger clusters, according to the hypothesis of Klots which states that any observed cluster comes from at least one dissociation: under this assumption, $Ag_5Br^+_4$ comes from two dissociation channels: (a) $Ag_6Br^+_5 \to Ag_5Br^+_4 + AgBr$ and (b) $Ag_8Br^+_7 \to Ag_5Br^+_4 + Ag_3Br_3$. The large abundance of $Ag_5Br^+_4$ is an indirect proof of the particular dissociation channel of $Ag_6Br^+_5$.

3.2.3 Fragmentation of non-stoichiometric clusters

The fragmentation channels have also been measured for some non-stoichiometric silver bromide clusters $Ag_nBr_{n-2,3,5}$ (Fig. 9). Once again, the neutral fragment is often Ag_3Br_3. The structure of these clusters has not been calculated and no detailed analysis can be done. Let us just point out another proof of the high stability of the metal-excess clusters since they often lose a stoichiometric fragment rather than their excess metal atoms.

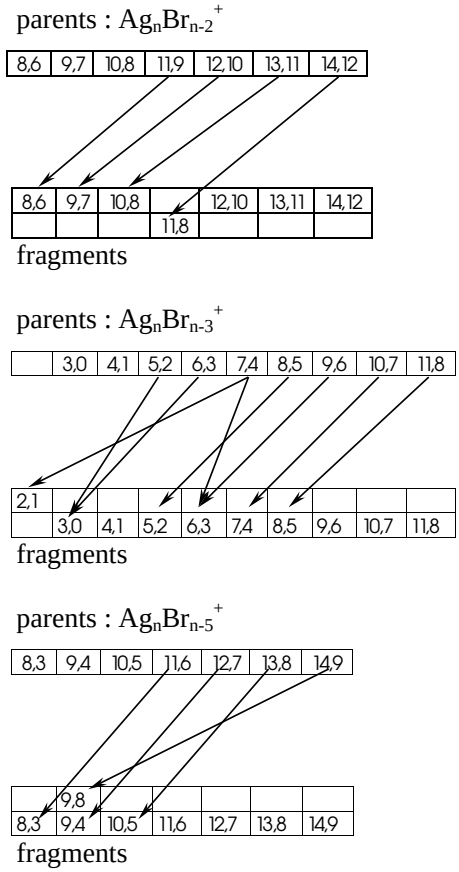

Fig. 9. Measured fragmentation channels of non-stoichiometric silver bromide cations: they often evaporate Ag_3Br_3. Each arrow represents an observed decay channel.

4 Comparison with other compounds of silver and copper

The copper halides are often considered as "covalent with a slightly ionic character" whereas silver halides are described as "ionic with a slightly covalent character". Even though the chemical properties of copper and silver are different in solution, their similar electronic shells ($...3d^{10}4s^1$ for copper, $...4d^{10}5s^1$ for silver) are likely to induce at least a few common properties of their compounds. We will show that our conclusions on silver bromide are helpful to understand at least two previously observed properties of copper and silver halides unexplained up to now. These properties are:

(1) the apparent particular stability of the trimer $(MX)_3$ and the large abundance of the trimer in their vapors;
(2) the quasi-planar (or at least cyclic) structure of their small stoichiometric clusters.

4.1 Gas phase

The vapor of all silver and copper halides surprisingly contains a large amount of trimers. The trimers are the main component of copper halides vapors in equilibrium with solid [26]. In the vapor of AgI in equilibrium with the solid phase at 750 K, the dimer and the trimer are roughly equally abundant [21]. The vapor of AgCl in equilibrium with the liquid phase at 820 K contains (AgCl) monomers (78%) and also trimers (22%) [22]. We do not know such quantitative results concerning AgBr, but its vapor is known to contain an important fraction of trimer $(AgBr)_3$ [26]. These results can obviously be related to our observation of the trimer as the main species evaporated by silver bromide clusters.

4.2 Clusters

First, let us notice that the mass spectra of small copper halide clusters $Cu_nX_{n-1}^+$, X = Cl, Br, I exhibit the same "magic numbers" ($n = 5$ and 14) as the spectrum of $Ag_nBr_{n-1}^+$ [27]. The $n = 14$ magic number is not a very specific signature because it is shared with a large number of other clusters, in particular with all ionic clusters. More interesting is the systematic large abundance of $M_5X_4^+$, whose origin (if the same as for silver bromide) may be closely related to the unusual stability and fragmentation pattern of this family of clusters (see Sect. 3.2.2). Beyond abundance spectra analysis, small $(MX)_n$ clusters (M = Cu, Ag, X = Cl, Br) trapped in an argon matrix have been investigated by infrared absorption spectroscopy in the eighties by Martin *et al.* [26, 27]. The vibrational frequencies calculated in the frame of a simple electrostatic model were compared with experiment. The copper chloride tetramer was experimentally demonstrated to be a square instead of the cubic ground state found in the calculations, although the energy of the square isomer was calculated to be 1.1 eV above the cube. The authors attributed this disagreement to entropy by taking into account its vibrational contribution to the free energy at high temperature. Let us recall that the ground state of $(AgBr)_4$ is also a cube in any electrostatic model, whereas it is a square in *ab initio* calculations. If one considers that the d electrons induce the same effects in copper halides as in silver bromide (these effects are detailed in [5]), there is no point in introducing entropy effects and the simplest way to interpret the measured vibrational spectrum of $(CuCl)_4$ is to consider the square as its electronic ground state. For larger copper bromide clusters $(CuBr)_{6,7,8}$, the measured vibrational spectra are not consistent with the 3D structures found in the model, but would be more easily understood as resulting from planar structures. Once again, this can be compared with recent calculations on AgBr for which the effect of d electrons is to constrain the ground state structures of stoichiometric clusters to remain two-dimensional at least up to $n = 6$ [5].

The preceding remarks can be extended to silver hydroxides. Mass spectrometry experiments have been carried out by Bréchignac and coworkers [23,24] on silver hydroxides. The main series observed are YX_n^+, where X is identified as $(AgOH)_3$. Although it is not fully understood, it clearly reveals the special role of the $(AgOH)_3$ substructure. *Ab initio* DFT calculation have been performed by

Millié and coworkers to determine the ground state geometry of $(AgOH)_n$ clusters. They found a particularly large binding energy for $(AgOH)_3$ [25]. Moreover, replacing Br by OH has no effect on the geometry: the structures of $(AgOH)_{2...6}$ are the same as those of $(AgBr)_{2...6}$ clusters.

5 Conclusion

Although silver bromide clusters can be considered at first order of approximation as ionic clusters if one consider only the $5s$ electrons of silver, we have experimentally demonstrated the indirect effects of the $4d$ orbitals of silver, which are responsible for a number of special features. The most unexpected is the preferential evaporation of $(AgBr)_3$. The lowest dissociation channels deduced from *ab initio* DFT calculations are in complete agreement with the experiment, and in particular is able to account for the singularity of $Ag_6Br_5^+$ that dissociates preferentially into $Ag_5Br_4^+ + AgBr$. This exception is responsible for the large abundance of $Ag_5Br_4^+$ in the mass spectra. Any calculation that does not account very carefully for the $4d$ electrons of silver fails to reproduce these results [5]. As far as there are not too many excess metal atoms, the cohesive energy given to the Ag^+–Ag^+ pairs by the $4d$ orbitals of silver, together with the known high cohesive energy of silver clusters [19,20], contributes significantly to the large stability observed for metal-rich clusters. By considering some particularities of silver bromide clusters as due to d electrons of silver, we are able to interpret some previously unexplained properties of isoelectronic systems MX, $M = Ag, Cu$, $X = Cl, Br, I, OH$. The preferential evaporation of trimers and the cyclic structures of small stoichiometric clusters are signatures of the partially covalent interaction in these systems. Even though it should be more deeply investigated both experimentally and theoretically, it seems that the common characters are due to a bonding interaction between the metal cations through their d orbitals.

References

1. P. Fayet, F. Granzer, G. Hegenbart, E. Moisar, B. Pischel, L. Wöste, Z. Phys. D **3**, 299 (1986).
2. M. Mostafavi, J.L. Marignier, J. Amblar, J. Belloni, Z. Phys. D **12**, 31 (1989).
3. J. Belloni, M. Treguer, H. Remita, R. De Keyzer, Nature **402**, 865 (1999).
4. R.W. Gurney, N.F. Mott, Proc. Roy. Soc. Lond. A **164**, 151 (1938).
5. F. Rabilloud, F. Spiegelmann, J.-M. L'Hermite, P. Labastie, J. Chem. Phys. **114**, 289 (2001).
6. O.K. Rice, H.C. Ramsperger, J. Am. Chem. Soc. **49**, 1617 (1927).
7. L.S. Kassel, J. Phys. Chem. **32**, 1065 (1928).
8. C.E. Klots, J. Chem. Phys. **83**, 5854 (1985).
9. P. Labastie, J.-M. L'Hermite, P. Poncharal, M. Sence, J. Chem. Phys. **103**, 6362 (1995).
10. Ph. Poncharal, J.-M. L'Hermite, P. Labastie, Chem. Phys. Lett. **253**, 463 (1996).
11. P. Labastie, J.-M. L'Hermite, P. Poncharal, L. Rakotoarisoa, M. Sence, Z. Phys. D **34**, 135 (1995).
12. J.-M. L'Hermite, L. Marcou, F. Rabilloud, P. Labastie, Rev. Sci. Ins. **71**, 2033 (2000).
13. I. Rabin, C. Jackschath, W. Shulze, F.W. Froben, Z. Phys. D **19**, 401 (1991).
14. P. Sharpe, C.J. Cassady, Chem. Phys. Lett. **191**, 111 (1992).
15. N.F. Mott, R.W. Gurney, *Electronic processes in ionic crystals*, 2nd edn. (Oxford Press, 1950).
16. F.C. Brown, *The physics of solid* (W.A. Benjamin, inc, 1967).
17. D. Rayane, R. Antoine, Ph. Dugourd, M. Broyer, J. Chem. Phys. (accepted for publication).
18. G. Durand, F. Spiegelmann, P. Poncharal, P. Labastie, J.-M. L'Hermite, M. Sence, J. Chem. Phys. **110**, 7884 (1999).
19. V. Bonačić-Koutecký, J. Pittner, M. Boiron, J. Chem. Phys. **110**, 3876 (1999) and references therein.
20. V. Bonačić-Koutecký, L. Češpiva, P. Fantucci, J. Kouteck, J. Chem. Phys. **98**, 7981 (1993).
21. M. Binnewies, H. Shäfer, Z. Anorg. Chem. **395**, 63 (1972).
22. M. Binnewies, K. Rinke, H. Shäfer, Z. Anorg. Chem. **395**, 51 (1972).
23. C. Bréchignac, Ph. Cahuzac, J. Leygnier, I. Tignères, Eur. Phys. J. D **9**, 421 (1999).
24. C. Bréchignac, Ph. Cahuzac, J. Leygnier, I. Tignères, Chem. Phys. Lett. **303**, 304 (1999).
25. M. Bertolus, V. Brenner, P. Millié, Eur. Phys. J. D **11**, 387 (2000).
26. T.P. Martin, H. Shaber, J. Chem. Phys. **73**, 3541 (1980).
27. T.P. Martin, A. Kakizaki, J. Chem. Phys. **80**, 3956 (1984).